International Journal of Nanomedicine

Dovepress
open access to scientific and medical research

Open Access Full Text Article

ORIGINAL RESEARCH

Synthesis of silver/montmorillonite nanocomposites using γ-irradiation

Kamyar Shameli[1]
Mansor Bin Ahmad[1]
Wan Md Zin Wan Yunus[1]
Nor Azowa Ibrahim[1]
Yadollah Gharayebi[2]
Sajjad Sedaghat[3]

[1]Department of Chemistry, Faculty of Science, Universiti Putra Malaysia, Selangor, Malaysia; [2]Department of Chemistry, Islamic Azad University Behbahan Branch, Iran; [3]Department of Chemistry, Islamic Azad University, Shahr-e Qods Branch, Tehran, Iran

Abstract: Silver nanoparticles (Ag-NPs) were synthesized into the interlamellar space of montmorillonite (MMT) by using the γ-irradiation technique in the absence of any reducing agent or heat treatment. Silver nitrate and γ-irradiation were used as the silver precursor and physical reducing agent in MMT as a solid support. The MMT was suspended in the aqueous $AgNO_3$ solution, and after the absorption of silver ions, Ag^+ was reduced using the γ-irradiation technique. The properties of Ag/MMT nanocomposites and the diameters of Ag-NPs were studied as a function of γ-irradiation doses. The interlamellar space limited particle growth (d-spacing [d_s] = 1.24–1.42 nm); powder X-ray diffraction and transmission electron microscopy (TEM) measurements showed the production of face-centered cubic Ag-NPs with a mean diameter of about 21.57–30.63 nm. Scanning electron microscopy images indicated that there were structure changes between the initial MMT and Ag/MMT nanocomposites under the increased doses of γ-irradiation. Furthermore, energy dispersive X-ray fluorescence spectra for the MMT and Ag/MMT nanocomposites confirmed the presence of elemental compounds in MMT and Ag-NPs. The results from ultraviolet-visible spectroscopy and TEM demonstrated that increasing the γ-irradiation dose enhanced the concentration of Ag-NPs. In addition, the particle size of the Ag-NPs gradually increased from 1 to 20 kGy. When the γ-irradiation dose increased from 20 to 40 kGy, the particle diameters decreased suddenly as a result of the induced fragmentation of Ag-NPs. Thus, Fourier transform infrared spectroscopy suggested that the interactions between Ag-NPs with the surface of MMT were weak due to the presence of van der Waals interactions. The synthesized Ag/MMT suspension was found to be stable over a long period of time (ie, more than 3 months) without any sign of precipitation.

Keywords: nanocomposites, silver nanoparticles, montmorillonite, γ-irradiation, powder X-ray diffraction

Introduction

Recently, metal nanoparticles (NPs) have stimulated worldwide investigation because of their remarkable physical and chemical properties relative to their bulk solid counterparts, due to their large proportion of high-energy surface atoms.[1] As a consequence, the production of NPs has attracted an enormous amount of attention in recent years. Silver NPs (Ag-NPs) have a number of superior properties and are widely used in different fields such as in medicine because of their antibacterial properties, in electronics as thick-film conductor conductivities, in surface-enhanced resonance Raman scattering, in optical biosensors, and in oxidative catalysis, photocatalysis, and chemical analysis.[2–9] In addition, nanosized silver colloid ink has recently been used for inkjet printing.[10] Recently, the investigation of the attractive antibacterial activities of Ag-NPs has reclaimed importance due to an increase of bacterial resistance

Correspondence: Kamyar Shameli
Department of Chemistry, Faculty of Science, Universiti Putra Malaysia, 43400 UPM Serdang, Selangor, Malaysia
Tel +60 3 89466793
Fax +60 3 89435380
Email kamyarshameli@gmail.com

submit your manuscript | www.dovepress.com
Dovepress
DOI: 10.2147/IJN.S15033

to antibiotics caused by their overuse. Presently, Ag-NPs displaying antibacterial activity are being synthesized. Antibacterial activity of the silver-containing materials can be used, for example, in medicine to reduce infections as well as to prevent bacterial colonization on prostheses, dental materials, vascular grafts, catheters, human skin, and stainless steel materials.[11] The Ag-NPs are normally short lived in aqueous solution as they agglomerate quickly. A sequence of elementary works by Henglein disclosed the reaction of colloidal silver in aqueous solutions.[12–14] Numerous methods have been utilized for the synthesis and stabilization of Ag-NPs. Problems with the stability of the produced colloidal Ag-NPs dispersions have been solved by the addition of polymers and surfactants.[15,16] Such complications do not occur if the NPs are deposited on a stable inert carrier. Ag-NPs have been deposited on glass,[17,18] alumina,[19] activated carbon,[20,21] glass fibers,[22] titanium nitride layers,[23] inorganic solid supports, and phyllosilicate clay as solid supports.[24–27] Thus, the preparation of Ag-NPs on solid supports such as phyllosilicate clays is a suitable way to prepare practically applicable supported particles as well as to control the particle size.[15,24] Phyllosilicate clays have an excellent swelling and adsorption ability, which are especially interesting for the impregnation of catalytically active nanosized metals in the interlamellar space of clay.[28,29] Therefore, exploring the possibility of using clays in developing metal supported catalysts is one of the main objectives of further efforts on clay investigation. As lamellar clay, montmorillonite (MMT) has intercalation, swelling, and ion exchange properties. In particular, its interlayer space has been used for the synthesis of material and biomaterial NPs as the support for anchoring transition metal complex catalysts and as adsorbents for cationic ions.[30,31] In addition, various production methods have been described for the synthesis of Ag-NP colloids using silver salt as the initial materials; for instance, chemical reduction,[32–35] aerosol spraying technique,[36] reverse micelle,[37] lamellar liquid crystal,[38] microemulsion,[39] micelle,[40] capping agent method,[41] and photochemical reduction (ie, microwave,[42] electron beam,[43] ultraviolet (UV)-irradiation,[44,45] and γ-irradiation).[46–48] Of these techniques, the use of γ-irradiation in the preparation of Ag-NPs has been demonstrated to have a number of highly advantageous properties compared with conventional chemical and photochemical methods, namely:

- The controlled reduction of silver ions can be carried out devoid of using surplus reducing agents or producing any undesired oxidation products from the reductants.
- The method provides Ag-NPs in completely reduced, extremely pure, and very stable states.
- The reducing agent is generated uniformly in the solution.
- The process is uncomplicated and uncontaminated.
- The γ-ray irradiation is harmless.
- No undesirable impurities similar to silver oxide are introduced.

Hence, based on our previous works, Ag-NPs in the interlayer space of MMT were synthesized by utilizing three different methods, ie, the chemical and physical reduction techniques by using β-D-glucose, $NaBH_4$, and the UV-irradiation method as the reducing agents.[15,24,32,44,45] Here, this article reports a simple γ-irradiation reduction method to synthesize the Ag-NPs in the interlayer space of MMT. This novel method in comparison to our other works, consist of controlled reduction without any undesired oxidation products, extremely stable colloids, very pure silver ions reduced to NPs in the high γ-irradiation doses. The Ag-NPs were intercalated into the lamellar space of phyllosilicate clay (MMT) utilizing γ-irradiation reduction in the absence of heat treatment or chemical reducing agents. Instead, MMT was used as the protective colloid, preventing the Ag-NPs from aggregation. Subsequently, it was found that MMT also assisted in the γ-reduction process of the Ag-NPs. At different γ-irradiation doses, both reduction and fragmentation of large Ag-NPs were found to have occurred simultaneously, and the particle size of the Ag-NPs decreased at high irradiation doses. Using this method, the researchers were able to obtain Ag-NPs of different sizes by controlling the γ-irradiation dose.

Materials and methods

Materials

All reagents in this work were of analytical grade and used as received without further purification. $AgNO_3$ (99.98%) was used as the silver precursor, which was obtained from Merck (Darmstadt, Germany). The MMT powder, applied as a solid support for Ag-NPs, was purchased as Kunipia-F (Kunimine Kogyo Co, Yamagata, Japan). All these aqueous solutions were used with double distilled water.

Synthesis of Ag/MMT nanocomposites by using γ-irradiation

For the synthesis of Ag/MMT nanocomposites, 5.0 g of MMT was dispersed in 400 mL double distilled water and vigorously stirred for 1 hour. One hundred milliliters of aqueous solution of $AgNO_3$ (0.2 mol/L) was added to the MMT aqueous suspension, and the mixture was further stirred for 1 hour. The mixture was then divided into five equal parts,

purged by N_2 for 30 minutes, and sealed. The suspension, which contained $AgNO_3$/MMT (A0), was irradiated under γ-irradiation source ^{60}Co with absorbed doses of 1, 5, 10, 20, and 40 kGy (A1–A5) at room temperature (ie, the dose rate at 67 Gy/min was calibrated using the Fricke dosimetry standard method). The produced Ag/MMT nanocomposite suspensions were brown and dark brown, depending on the absorbed doses. The suspensions of the Ag/MMT nanocomposites were then retrieved by centrifugation at the speed of 15,000 rpm for 20 minutes, washed with double distilled water twice to remove residue $AgNO_3$, and dried overnight under vacuum.

Characterization methods and instruments

The prepared Ag/MMT nanocomposites were characterized by using powder X-ray diffraction (PXRD), transmission electron microscopy (TEM), scanning electron microscopy (SEM), energy dispersive X-ray fluorescence (EDXRF) spectrometry, UV-visible spectroscopy, and Fourier transform infrared (FT-IR) spectroscopy. The changes in the interlamellar spacing of MMT and Ag/MMT nanocomposites were also studied using PXRD in the angle range of $2° < 2\theta < 12°$. In addition, the interlamellar space was calculated based on the PXRD peak positions using Bragg's equation. A wavelength (λ) of 0.15418 nm was used for these measurements. The PXRD patterns were recorded at a scan speed of 2° per minute. The structures of the produced Ag/MMT nanocomposites were examined using PXRD-6000 (Shimadzu, Kyoto, Japan). TEM observations were carried out using the H-7100 electron microscope (Hitachi, Tokyo, Japan), and the particle size distributions were determined using UTHSCSA Image Tool software (version 3.00; UTHSCSA Dental Diagnostic Science, San Antonio, TX). The SEM was performed using the XL-30 instrument (Philips, Amsterdam, The Netherlands) to study the morphology of MMT and Ag/MMT nanocomposites (A1–A5). EDXRF was carried out on a EDX-700HS spectrometer (Shimadzu). The UV-visible spectra were recorded over the range of 300–700 nm using the H.UV.1650 PC UV-visible spectrophotometer (Shimadzu). The elemental analysis of as-synthesized Ag-NPs was quantified by using an inductively coupled plasma-optical emission spectrophotometer (ICP-OES) model Optima 2000DV (PerkinElmer, Waltham, MA). The FT-IR spectra were recorded over the range of 400–4000 cm^{-1} using a Series 100 FT-IR 1650 spectrophotometer (PerkinElmer). After the reactions, the samples were centrifuged by using a high-speed centrifuge machine (Avanti J25; Beckman, Brea, CA).

Results

The synthesis of Ag/MMT nanocomposites from $AgNO_3$/MMT produced by γ-irradiation reduction is depicted schematically in Figure 1. During the γ-irradiation, both reduction and fragmentation of large Ag-NPs were found to have occurred simultaneously. The small Ag-NPs were intercalated into the lamellar space of MMT using γ-irradiation reduction in the absence of chemical reducing agents or heat treatment. The color of the prepared

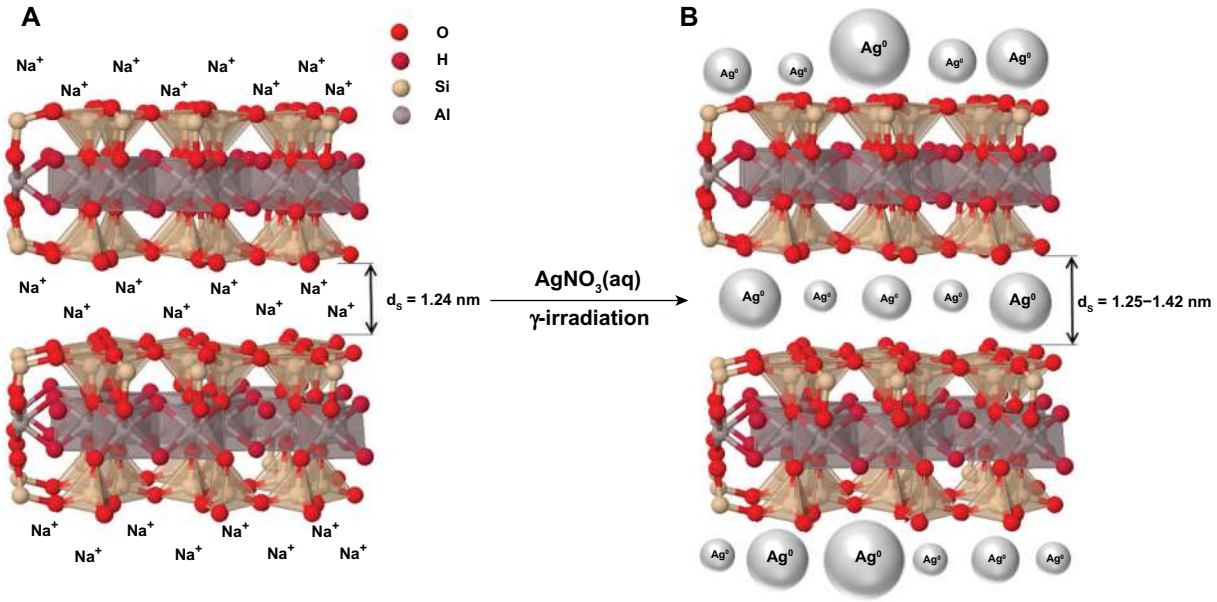

Figure 1 Schematic illustration of the synthesis of the silver nanoparticles on montmorillonite suspension by γ-irradiation doses.

samples at different γ-irradiation doses gradually changed from colorless for $AgNO_3$/MMT suspension (A0) to brown (A1, A2), and finally to dark brown (A3–A5), depending on the absorbed doses, indicating the formation of Ag-NPs in the MMT suspension (Figure 2). The comparison between the PXRD patterns of the MMT and Ag/MMT nanocomposites (A1–A5) in the small angle range of 2θ ($2° < 2\theta < 12°$) indicated the formation of the intercalated Ag-NPs structure (Figure 3). The PXRD peaks in the wide angle range of 2θ ($30° < 2\theta < 80°$) ascertained that the peaks in 38.34°, 44.41°, 64.37°, and 77.65° related to the 111, 200, 220, and 311 crystalline structures of the face-centered cubic (fcc) synthesized silver nanocrystal, respectively (Figure 4). The TEM images and their size distribution of Ag-NPs demonstrated that with the increased γ-irradiation doses, the mean diameters of Ag-NPs gradually increased to 21.57, 24.75, 27.70, and 30.63 nm for 1, 5, 10, and 20 kGy, but then decreased to 28.56 nm in 40 kGy due to the large size fragmentation of Ag-NPs at a high dose of γ-irradiation (Figure 5). The SEM images indicated that there were surface structure changes between the initial MMT and Ag/MMT nanocomposites under different doses of γ-irradiation. Moreover, with the increased γ-irradiation doses in the exterior morphology of Ag/MMT nanocomposites, large flakes of layered MMT changed to small flakes with increased holes in the surfaces of Ag/MMT layers. Additionally, the EDXRF spectra for the MMT and Ag/MMT nanocomposites (with 1, 10, 20, and 40 kGy, respectively) confirmed the presence of elemental compounds in MMT and Ag-NPs without any other impurity peaks (Figure 6). The formation of Ag-NPs was also followed by the measurement of the surface plasmon resonance (SPR) bands of the $AgNO_3$/MMT and Ag/MMT nanocomposite suspensions at the wavelengths ranging from 300 to 700 nm (Figure 7). The chemical characterizations of the as-synthesized Ag-NPs in MMT were done using the ICP-OES analyzer. The results from the ICP-OES analysis showed that the formation of Ag-NPs increased at higher γ-irradiation doses (Table 1). Furthermore, the FT-IR spectra (Figure 8) showed the existence of van der Waals interactions between the silicate layers and Ag-NPs in the Ag/MMT nanocomposites. The stability of the synthesized MMT suspensions containing Ag-NPs was analyzed by storing the samples at room temperature (~25°C) for more than 3 months. The absorbance at 360–415 nm was monitored at a period of 24 hours to check for agglomeration. No significant change in the absorbance was noticed during storage, representing a good stability of Ag-NPs in the MMT suspension.

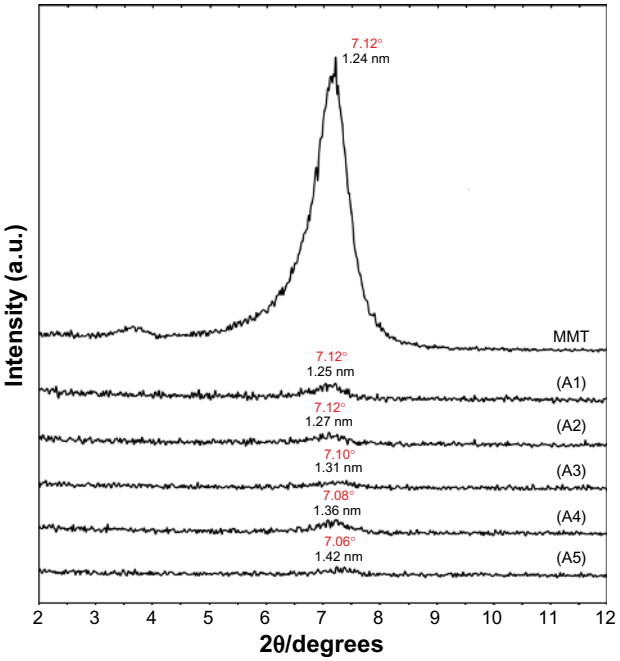

Figure 3 Powder X-ray diffraction patterns of montmorillonite (MMT) and Ag/MMT nanocomposites for 1, 5, 10, 20, and 40 kGy (A1–A5).

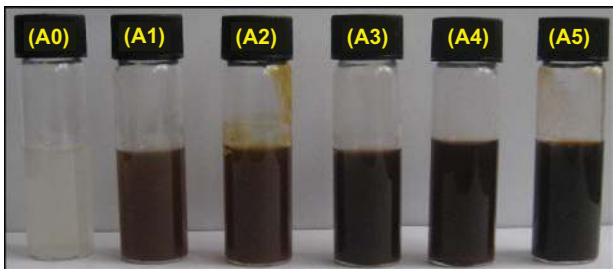

Figure 2 Photograph of $AgNO_3$/MMT (A0) and Ag/MMT nanocomposite suspensions at different γ-irradiation doses: 1, 5, 10, 20, and 40 kGy (A1–A5).
Abbreviation: MMT, montmorillonite.

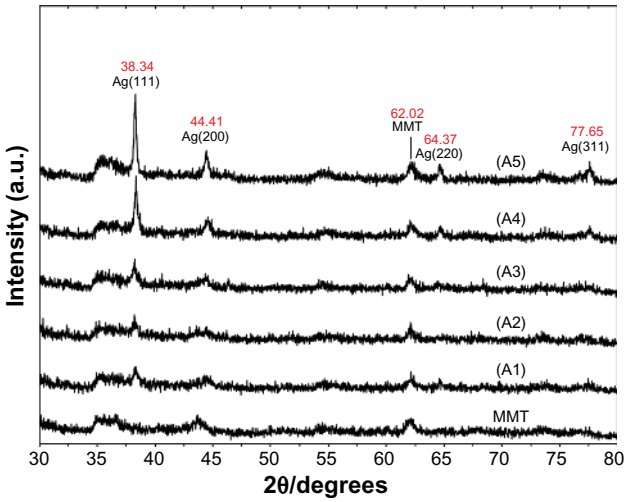

Figure 4 Powder X-ray diffraction patterns of montmorillonite (MMT) and Ag/MMT nanocomposites at the different γ-irradiation doses: 1, 5, 10, 20, and 40 kGy (A1–A5).

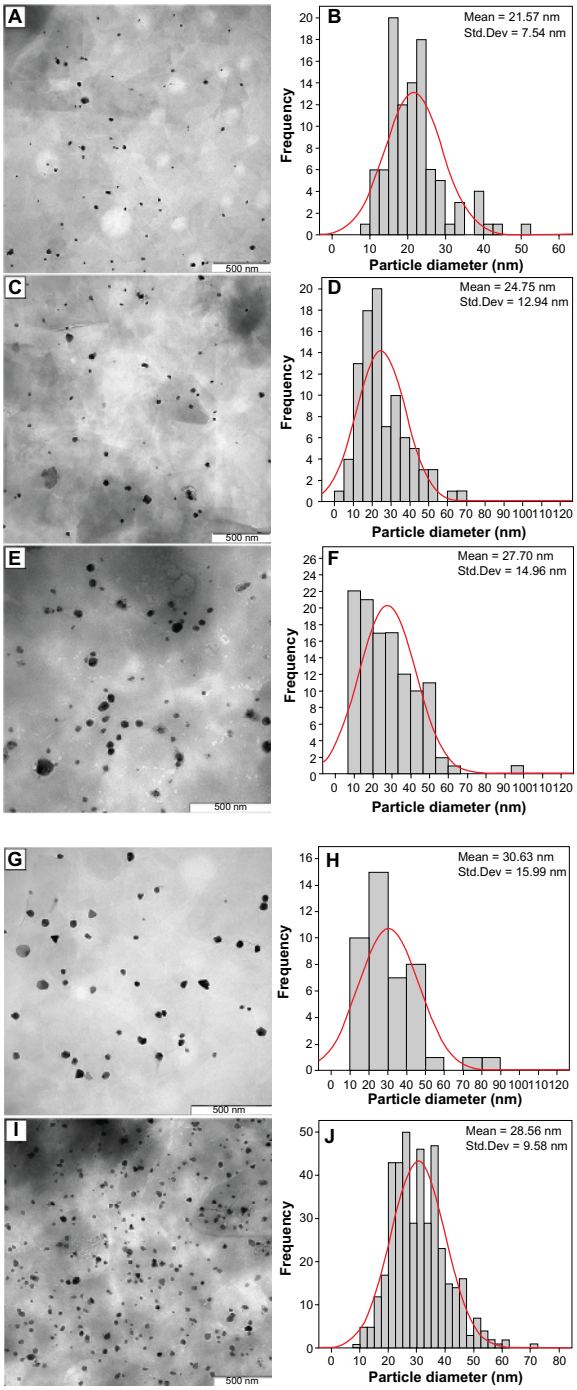

Figure 5 TEM images and their corresponding particle size distributions of Ag/MMT nanocomposites at the different γ-irradiation doses: 1 kGy (**A, B**), 5 kGy (**C, D**), 10 kGy (**E, F**), 20 kGy (**G, H**), and 40 kGy (**I, J**).
Abbreviations: MMT, montmorillonite; TEM, transmission electron microscopy.

Discussion

There have been numerous studies on the γ-induced reduction of Ag-NPs in aqueous and other solutions. In this method, $AgNO_3$/MMT aqueous suspensions were exposed to γ-rays creating hydrated electrons and primary radicals and molecules as described in Equation 1.[49,50]

$$H_2O \xrightarrow{\gamma\text{-Ray}} e^-_{aq} + H^{\bullet} + OH^{\bullet} + H_3O^+ + H_2 + H_2O_2 + \cdots, \quad (1)$$

$AgNO_3$ separated to Ag^+ and NO_3^- ions in the aqueous solution as shown in Equation 2. The solvated electrons, ie, e^-_{aq}, and H atoms are strong reducing agents; therefore, in the following step, they easily reduced silver ions down to the zero-valent state (Equations 3 and 4):[51]

$$AgNO_3 \rightarrow Ag^+ + NO_3^- \quad (2)$$

$$Ag^+ + e^-_{aq} \xrightarrow{\text{reduction}} Ag^0 \quad (3)$$

$$Ag^+ + H^{\bullet} \xrightarrow{\text{reduction}} Ag^0 + H^+ \quad (4)$$

Silver atoms formed by the irradiation tended to coalesce into oligomers (Equation 5), which progressively grew into large clusters (Equation 6). The aqueous electrons reacted with the Ag^+ clusters to form the relatively stabilized Ag clusters (Equation 7).[52,53]

$$Ag^0 + Ag^+ \rightarrow Ag_2^+ \quad (5)$$

$$nAg^+ + Ag_2^+ \rightarrow (Ag)_n^+ \quad (6)$$

$$(Ag)_n^+ + ne_{aq} \rightarrow (Ag)_n \quad (7)$$

γ-induced fragmentation of Ag nanocluster $[(Ag)_n]$ occurred at a high dose of γ-irradiation (40 kGy).[54,55] This can be summarized through a biphotonic process, as shown in Equations 8 and 9.

$$(Ag)_n \xrightarrow{\gamma\text{-Ray}} (Ag)_n^+ + ne^-_{aq} \quad (8)$$

$$(Ag)_n^+ \xrightarrow{\gamma\text{-induce fragmentation}} (Ag)_{n-1} + Ag^+, \quad (9)$$

where $(Ag)_n$ is the silver nanocluster containing n silver atoms, and e^-_{aq} is the aqueous electron. After the γ-irradiation of the aqueous suspension of $AgNO_3$/MMT, a large amount of aqueous electrons (e^-_{aq}) was produced, and the Ag^+ ions were reduced into Ag-NPs.

X-ray diffraction

The original d-spacing (d_S) of MMT (1.24 nm) in the Ag/MMT nanocomposites (A1–A5) was increased to 1.25, 1.27, 1.31, 1.36, and finally 1.42 nm at the 2θ angles of 7.12°, 7.12°, 7.10°, 7.08°, and 7.06°, respectively (Figure 3). These d_S values were direct proof of the nanosilver intercalation structures between the interlayer spaces of MMT. Meanwhile, the Ag-NPs formed at the latter location were the causes of the increase in the basal spacing. In these samples, the intensities of the reflections were significantly lower, whereas

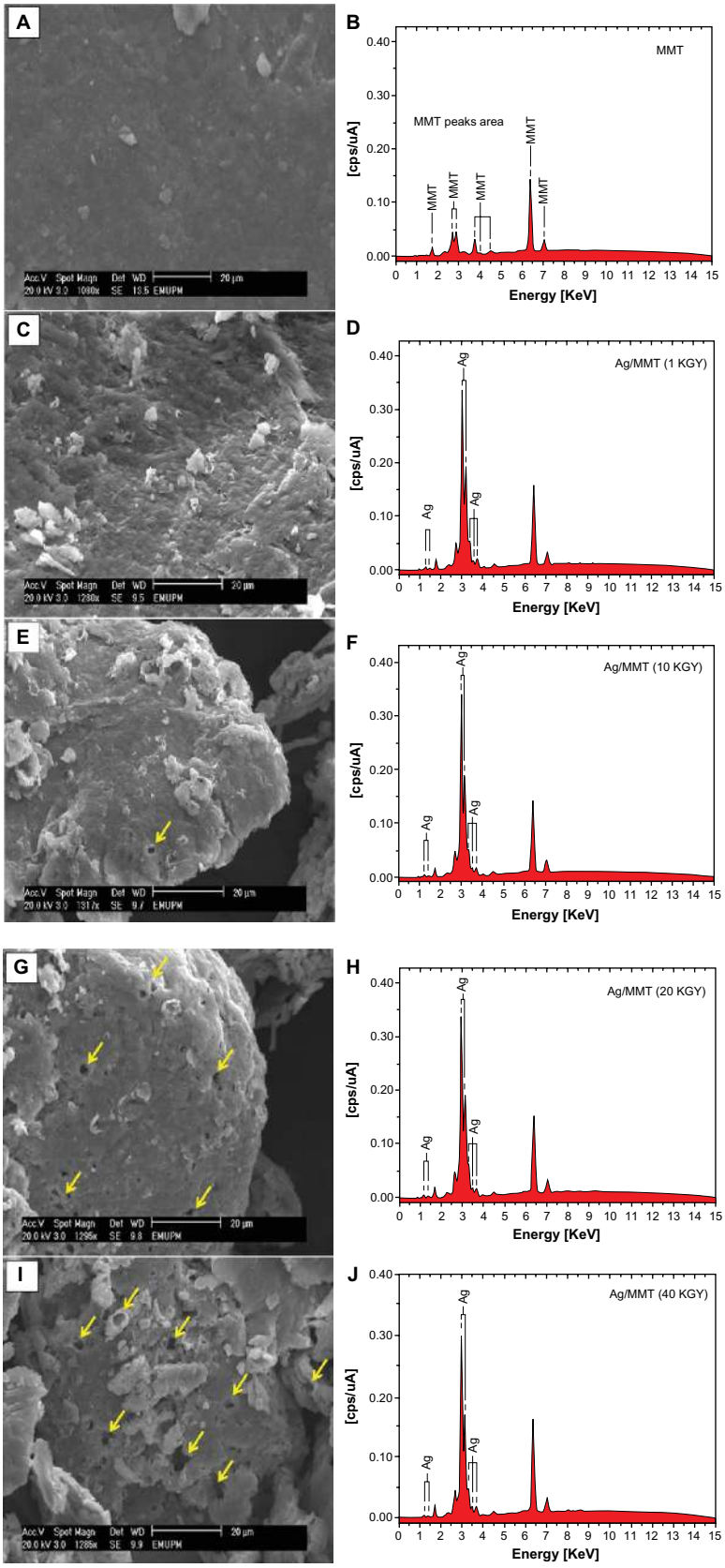

Figure 6 SEM micrographs and EDXRF spectra respectively for the MMT (**A, B**) and Ag/MMT nanocomposites: 1 kGy (**C, D**), 10 kGy (**E, F**), 20 kGy (**G, H**), and 40 kGy (**I, J**).
Abbreviations: EDXRF, energy dispersive X-ray fluorescence; MMT, montmorillonite; SEM, scanning electron microscopy.

their half-widths were larger than the undoped clay minerals, whereby the highly ordered parallel lamellar structure of the mineral was disrupted by the metal NP formation.[26] In addition, all the Ag/MMT nanocomposites (A1–A5) had a similar diffraction profile, and the PXRD peaks at 2θ of 38.34°, 44.41°, 64.37°, and 77.65° (Figure 4) could be attributed to 111, 200, 220, and 311 crystallographic planes of the fcc silver crystals, respectively.[56] For all the samples, the main crystalline phase was silver, while no obvious other phases (impurities) were found in the PXRD patterns (PXRD Ref. No. 01-087-0718). Moreover, the PXRD peak broadenings of Ag-NPs were mostly due to the existing nanosized particles in the nanocomposites.[57] In addition, there was also a characteristic peak at about 2θ = 62.02°, which related to the MMT clay (PXRD Ref. No. 00-003-0010) as a stable substrate. The intensities of 111, 200, 220, and 311 reflections due to the Ag NP phase were also found to increase along with the increased Ag NP content in several γ-irradiation doses.

Morphology

The TEM images and their corresponding particle size distributions of Ag-NPs in MMT suspensions at different γ-irradiations are shown in Figure 5. When the $AgNO_3$/MMT suspension was irradiated under γ-ray with 1 kGy dose, γ-reduced Ag-NPs were formed with a (mean diameter and standard deviation of about 21.57 ± 7.54 nm) (Figure 5A and 5B). When the γ-irradiation doses were increased to 5, 10, and 20 kGy, the mean diameter and standard deviation of Ag-NPs gradually increased to 24.75 ± 12.94 nm, 27.70 ± 14.96 nm, and 30.63 ± 15.99 nm (Figure 5C–5H). Due to the presented layer structure of MMT, as a solid support, and the absorption of silver ions between these layers, large Ag-NPs were gradually obtained in these interlayer spaces with the increase of γ-irradiation doses from 1 kGy to 20 kGy. However, the observation was consistent with earlier findings by other researchers who had reported that small Ag-NPs were obtained under further γ-irradiation doses at 40 kGy, with the mean diameter and standard deviation of 28.56 ± 9.58 nm for A5 (Figure 5I and 5J).[58] The result showed a narrow size distribution of the Ag-NPs, indicating that the particles after 40 kGy were highly homogeneous (Table 1). This result also indicated that the interlayer structure of the MMT suspension, with the increased γ-irradiation doses, gradually solvated e^-_{aq} electron concentration, which were increased in the solvent.[51] Therefore, Ag-NPs between the layers of MMT slowly prepared and increased the particle size and standard deviation from 1 to 20 kGy. When the dose of irradiation was increased to 40 kGy, the γ-induced fragmentation of large flakes of MMT layers and large Ag-NPs gradually commenced. The SEM images of MMT and Ag/MMT nanocomposites (A1, A3, A4, and A5) are presented in Figure 6. Moreover, the surface morphology of MMT demonstrated a layered surface with some large flakes, which is a typical structure of MMT (Figure 6A). The exterior morphology of Ag/MMT nanocomposites demonstrated short flakes and big holes in the exterior surface of the Ag/MMT nanocomposites, which increased with increasing γ-irradiation dose (1–40 kGy). Furthermore, with the increase of irradiation, the external surfaces of the Ag/MMT nanocomposites were shiny due to the presence of Ag-NPs (Figure 6A, 6C, 6E, 6J, and 6H). The EDXRF spectra for MMT and Ag/MMT nanocomposites are demonstrated in Figure 6B, 6D, 6F, and 6H. The peaks around 1.7, 2.6, 2.8, 3.6, 4.5, 6.4, and 7.1 keV were related to the binding energies of MMT, whereas the peaks around 1.2, 1.4, 3.1, 3.2, 3.4, 3.5, and 3.7 keV related to the silver elements in A1, A3–A5, respectively.[59] Additionally, the EDXRF spectra for MMT and the Ag/MMT nanocomposites confirmed the presence of elemental compounds in MMT and Ag-NPs without any impurity peaks. The results indicated that the synthesized nanocomposites were composed of high-purity Ag-NPs.

UV-visible spectroscopy

The UV-visible absorption spectra of MMT based on Ag-NPs prepared by γ-irradiation are shown in Figure 7. Notably, the characteristic of the silver SPR bands were detected in the range of 360–415 nm. These absorption bands were presumably corresponding to the Ag-NPs smaller than 30 nm.[60] However, there was no characteristic of UV-visible absorption of Ag-NPs before the γ-irradiation for the $AgNO_3$/MMT suspension (A0). The UV-visible spectra of the samples showed that after irradiation at 1 kGy, a low-intensity peak appeared at 360 nm, indicating the formation of Ag-NPs with low concentration (A1). With the increased dose of γ-irradiation from 5 to 10 and 20 kGy, the intensity of the absorption band increased significantly with their position doses changed noticeably at 390, 408, and 415 nm, respectively. These absorption bands were broad and red-shifted to high wavelengths (A2–A4). It was also observed that, at higher doses of γ-irradiation, the γ-induced fragmentation of NPs in the solid support matrix had increased (Table 1). Therefore, the SPR band absorption peak tended to undergo a blue-shift to 413 nm, with continuously increasing the dose of γ-irradiation to 40 kGy.[58] The increase of the absorbance with increased dose

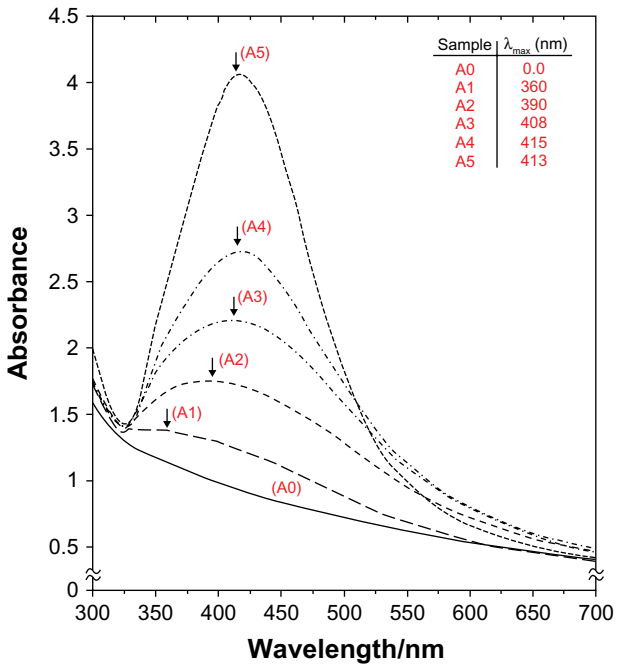

Figure 7 UV-visible absorption spectra for $AgNO_3$/MMT (A0) and Ag/MMT nanocomposites suspension at the different γ-irradiation doses: 1, 5, 10, 20, and 40 kGy (A1–A5).
Abbreviations: MMT, montmorillonite; UV, ultraviolet.

of γ-irradiation indicated that the concentration of Ag-NPs also increased.[61]

Inductively coupled plasma-optical emission spectroscopy

To determine the approximate efficiency of $AgNO_3$/MMT suspension of γ-induced reduction to Ag/MMT nanocomposites, the ICP-OES analyzer was used in this study. A modified digestion method was used to quantify the amount of Ag NP conversion to Ag^+ in the MMT. An air-dry mass of each Ag/MMT nanocomposite (A1–A5) was submerged in a solution of 10 mL of ultrapure reagent-grade nitric acid (>90%, 364576; Sigma-Aldrich, St. Louis, MO) and 10 mL of double distilled water. After an observation glass was placed over the digestion beaker, the solution was heated to approximately 80°C for 15 minutes and allowed to react. The digestion solution was allowed to cool and then filtered through a glass fiber filter (Qualitative #2; Whatman, Florham Park, NJ) and diluted to 100 mL in a volumetric flask.[62] Using ICP-OES spectroscopy to detect the silver ions, the approximate efficiency gradually increased from 8.31% to 19.05%, 37.35%, 45.54%, and finally 56.15% after 1, 5, 10, 20, and 40 kGy of γ-irradiation, respectively (Table 1). The increase of the approximate efficiency with increasing doses of γ-irradiation demonstrated that the yield of Ag-NPs also increased.

FT-IR chemical analysis

Figure 8 shows the comparison of FT-IR spectra for the silicate structure of MMT and Ag/MMT with different doses of γ-irradiation. The position of vibration bands in the region of 3635 cm^{-1} corresponded to O–H stretching, 3442 cm^{-1} due to the interlayered O–H stretching (H bonding) at 1650 and 1526 cm^{-1} for H–O–H bending. The bands at 1127, 1010, and 910 cm^{-1} were also assigned to the stretching vibration of Si–O, which was usually taken as evidence for a three-dimensional amorphous silica phase.[63] The band at 628 cm^{-1} was due to Al–OH, and 910 cm^{-1} was due to (Al, Mg)–OH. The band at 521–433 cm^{-1} was assigned to Si–O–Si bending vibration.[64] The FT-IR spectra indicated the rigidity of silicate layers and nonbond chemical interaction between the silicate layers and Ag-NPs in Ag/MMT nanocomposites. The interactions between the silicate layers of MMT and Ag-NPs were associated with the peak at 3442 cm^{-1}. Broad peak was due to the presence of van der Waals interactions between the hydroxyl groups of MMT layers and the partial positive charge on the surface of Ag-NPs.[65] These peaks, with the

Table 1 Physical properties of Ag-NPs in Ag/MMT nanocomposites synthesized at different γ-irradiation doses in a constant concentration (0.2 mol/L) of $AgNO_3$

Sample	γ-irradiation dose (kGy)	λ_{max} [a]	Absorbance[b]	Approximated efficiency (%)	Ag NP particle size[c] (nm)
A1	1	360	0.68	8.31 ± 0.42	21.57 ± 7.54
A2	5	390	0.83	19.05 ± 0.47	24.75 ± 12.94
A3	10	408	1.06	37.35 ± 0.51	27.20 ± 14.96
A4	20	415	1.45	45.54 ± 0.68	30.64 ± 15.99
A5	40	413	2.08	56.15 ± 0.71	28.56 ± 9.58

Notes: [a]The experiments were repeated three times, and they were averaged to give the data in this table; [b]The data were obtained by multiplying the absorbance of the corresponding diluted solutions by their dilution factors when diluted solutions were used for the data; [c]The size of the Ag-NPs was determined by measuring diameters of about 100 NPs in TEM image and averaging them.
Abbreviations: MMT, montmorillonite; NP, nanoparticle; TEM, transmission electron microscopy.

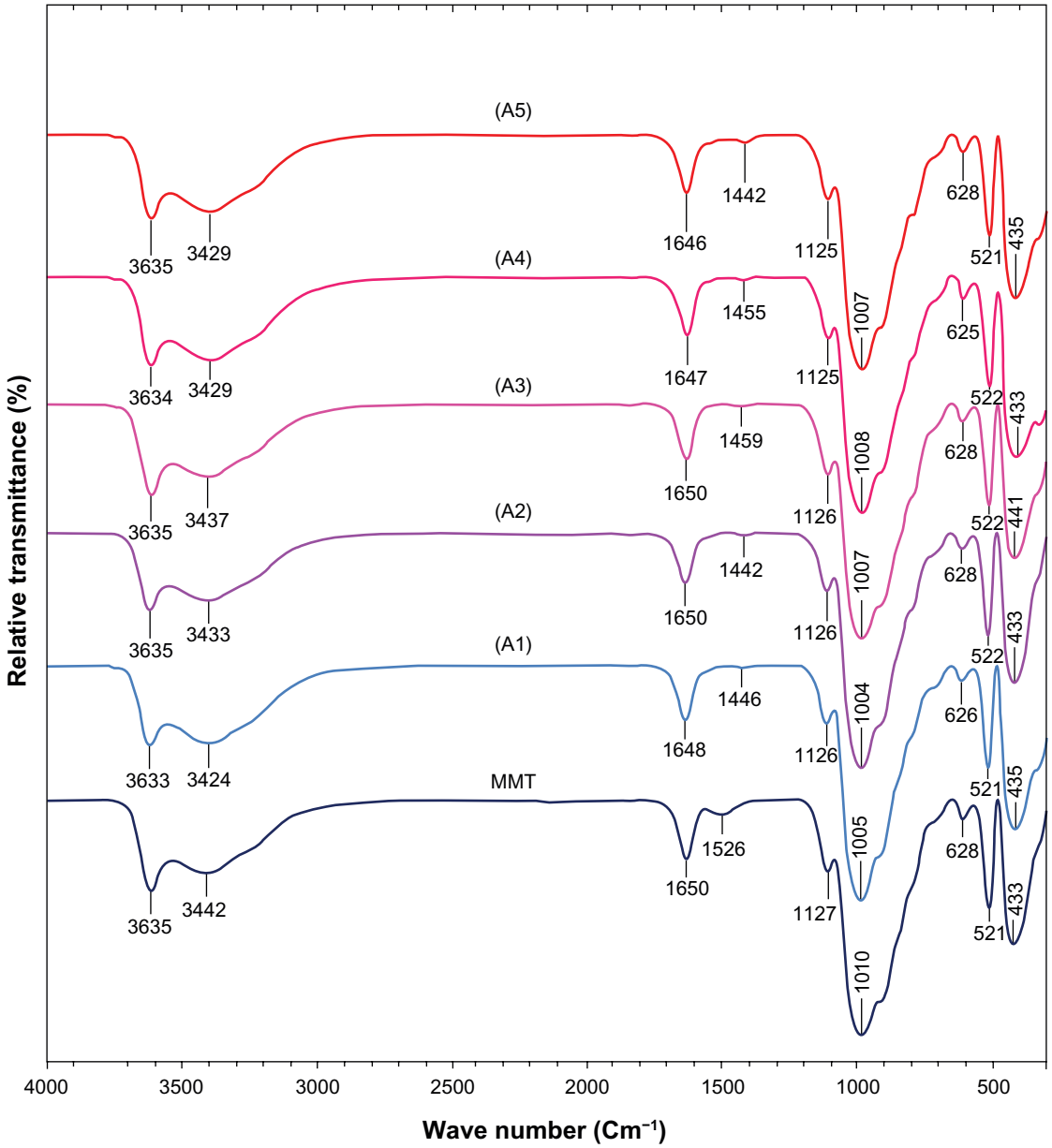

Figure 8 FT-IR spectra of montmorillonite (MMT), Ag/MMT nanocomposites at the different γ-irradiation doses: 1, 5, 10, 20, and 40 kGy (A1–A5).
Abbreviation: FT-IR Fourier transform infrared.

enhanced Ag-NPs, as a result of the increased γ-irradiation doses for all samples, shifted to low wave numbers, and the peak intensity was decreased.

Conclusion

In summary, the Ag-NPs were successfully prepared from the $AgNO_3$/MMT suspension by using the γ-irradiation induced method with the absorbance doses of 1–40 kGy in the interlamellar space of MMT at room temperature without any reducing agent. These Ag-NPs were found to be stabilized by the interlayer space of MMT as a solid support. The PXRD patterns in the small angle range of 2θ ($2° < 2θ < 12°$) showed that the interlamellar space limited the particle growth for the formation of the intercalated Ag-NP structures. In the wide angle range of 2θ ($30° < 2θ < 80°$), the PXRD patterns ascertained that the crystalline structures of Ag-NPs for all samples were fcc. The results from TEM demonstrated that with the increased γ-irradiation doses, the particle diameters of the Ag-NPs gradually increased from 1 to 20 kGy; however, after higher doses at 40 kGy, the particle diameters decreased suddenly as a result of the increased γ-induced fragmentation in Ag-NPs. The SEM images demonstrated large-layered surface of the MMT and short-flaked surface with big holes in the exterior surface of

Ag/MMT nanocomposites, which increased with increasing γ-irradiation dose. Moreover, the EDXRF spectra for the Ag/MMT nanocomposites confirmed the presence of elemental compounds in MMT and Ag-NPs without any contamination peaks. The UV-visible absorption spectra showed the peak characteristic of the SPR bond of Ag-NPs, which were detected in the ranges of 360–415 nm for 1–20 kGy and 413 nm for 40 kGy because the γ-induced fragmentation of Ag-NPs had increased. Therefore, the maximum absorbance shifted to low wavelength (blue-shift). In addition, the increase of the absorbance with further γ-irradiation doses indicated that the concentration of Ag-NPs also increased. The ICP-OES analysis demonstrated that the formation of Ag-NPs in MMT increased at higher γ-irradiation doses. Moreover, FT-IR suggested that the interactions between Ag-NPs with the surface of MMT were weak due to the presence of van der Waals interactions. The synthesized Ag/MMT suspensions were found to be stable over a long time without any sign of precipitation.

Acknowledgments

The authors are grateful to the staff of the Department of Chemistry, Institute of Bioscience of University Putra Malaysia, and also Mrs Parvaneh Shabanzadeh who had contributed to this work. The contribution of the Malaysian Nuclear Agency staff for irradiation facility is appreciated.

Disclosure

The authors have no conflicts of interest to disclose in this work.

References

1. Murphy CJ. Materials science. Nanocubes and nanoboxes. *Science*. 2002;298(5601):2139–2141.
2. Shameli K, Ahmad MB, Yunus WMZW, et al. Silver/poly (lactic acid) nanocomposites: preparation, characterization, and antibacterial activity. *Int J Nanomedicine*. 2010;5:573–579.
3. Ahmad MB, Shameli K, Darroudi M, et al. Antibacterial activity of silver/clay/chitosan bionanocomposites. *Res J Biol Sci*. 2009;4(11): 1156–1161.
4. Chang LT, Yen CC. Studies on the preparation and properties of conductive polymers. VIII. Use of heat treatment to prepare metallized films from silver chelate of PVA and PAN. *J Appl Polym Sci*. 1995;55: 371–374.
5. Faulds K, Smith WE, Graham D. Evaluation of surface-enhanced resonance raman scattering for quantitative DNA analysis. *Anal Chem*. 2003;76:412–417.
6. Haes AJ, Zou S, Schatz GC, et al. Nanoscale optical biosensor: short range distance dependence of the localized surface plasmon resonance of noble metal nanoparticles. *J Phys Chem B*. 2004;108: 6961–6968.
7. Sclafani A, Herrmann J. Influence of metallic silver and of platinum-silver bimetallic deposits on the photocatalytic activity of titania (anatase and rutile) in organic and aqueous media. *J Photochem Photobiol A*. 1998;113(2):181–188.
8. Shiraishi Y, Toshima N. Oxidation of ethylene catalyzed by colloidal dispersions of poly(sodium acrylate)-protected silver nanoclusters. *Colloids Surf A Physicochem Eng Asp*. 2000;169:59–66.
9. Sherrod SD, Diaz AJ, Russell WK, et al. Silver nanoparticles as selective ionization probes for analysis of olefins by mass spectrometry. *Anal Chem*. 2008;80:6796–6799.
10. Lee HH, Chou KS, Huang KC. Inkjet printing of nanosized silver colloids. *Nanotechnology*. 2005;16:2436–2441.
11. Panacek A, Kvitek L, Prucek R, et al. Silver colloid nanoparticles: synthesis, characterization, and their antibacterial activity. *J Phys Chem B*. 2006;110:16248–16253.
12. Henglein A. Electrochemical reactions of some organic free radicals at colloidal silver in aqueous solution. *J Phys Chem*. 1980;84: 3461–3467.
13. Henglein A. Small-particle research: physicochemical properties of extremely small colloidal metal and semiconductor particles. *Chem Rev*. 1989;89:1861–1873.
14. Henglein A. Reduction of $Ag(CN)_2$ on silver and platinum colloidal nanoparticles. *Langmuir*. 2001;17:2329–2333.
15. Ahmad MB, Shameli K, Yunus WMZW, et al. Synthesis and characterization of silver/clay/starch bionanocomposites by green method. *Aust J Basic Appl Sci*. 2010;4(7):2158–2165.
16. Sadjadia MAS, Sadeghia B, Meskinfam M. Synthesis and characterization of Ag/PVA nanorods by chemical reduction method. *Physica E*. 2008;40:3183–3186.
17. Li W, Seal S, Megan E, et al. Physical and optical properties of sol-gel nano-silver doped silica film on glass substrate as a function of heat-treatment temperature. *J Appl Phys*. 2003;93:9553–9561.
18. Nahal A, Shapoori K. Linear dichroism, produced by thermo-electric alignment of silver nanoparticles on the surface of ion-exchanged glass. *Appl Surf Sci*. 2009;255:7946–7950.
19. Esteban CA, Díaz C, Fernández A, et al. Silver nanoparticles supported on α-, η- and δ-alumina. *J Eur Ceramic Soc*. 2006;26(1–2):1–7.
20. Yoon KY, Byeon JH, Park CW, et al. Antimicrobial effect of silver particles on bacterial contamination of activated carbon fibers. *Environ Sci Technol*. 2008;42(4):1251–1255.
21. Sawai O, Oshima Y. Deposition of silver nanoparticles on activated carbon using supercritical water. *J Supercrit Fluids*. 2008;47(2): 240–246.
22. Sharifi N, Taghavinia N. Silver nano-islands on glass fibers using heat segregation method. *Mater Chem Phys*. 2009;113:63–66.
23. Akhavan O. Silver nanocube crystals on titanium nitride buffer layer. *J Phys D: Appl Phys*. 2009;42:105305–105311.
24. Ahmad MB, Shameli K, Darroudi M, et al. Synthesis and characterization of silver/clay nanocomposites by chemical reduction method. *Am J Appl Sci*. 2009;6(11):1909–1914.
25. Ayyappan S, Subbanna GN, Goplan RS, et al. Nanoparticles of nickel and silver produced by the polyol reduction of the metal salts intercalated in montmorillonite. *Solid State Ionic*. 1996;84:271–281.
26. Patakfalvi RA, Oszka A, Dekany I. Synthesis and characterization off silver nanoparticles/Kaolinite composites. *Colloid Surfaces Physicochem Eng Aspect*. 2003;220:45–54.
27. Valášková M, Martynková GS, Lešková J, et al. Silver nanoparticles/montmorilloniet composites prepared using nitrating reagent at water and glycerol. *J Nanosci Nanotechnol*. 2008;8:1–9.
28. Manikandan D, Divakar D, Rupa AV, et al. Synthesis of platinum nanoparticles in montmorillonite and their catalytic behavior. *Appl Clay Sci*. 2007;37(1–2):193–200.
29. Miao S, Liu Z, Han B, et al. Ru nanoparticles immobilized on montmorillonite by ionic liquids: a highly efficient heterogeneous catalyst for the hydrogenation of benzene. *Angew Chem Int Edit*. 2005;45(2): 266–269.
30. Belova V, Möhwald H, Shchukin DG. Sonochemical intercalation of preformed gold nanoparticles into multilayered clays. *Langmuir*. 2008; 24:9747–9753.
31. Paek SM, Jang JU, Hwang SJ, et al. Exfoliation-restacking route to Au nanoparticle-clay nanohybrids. *J Phys Chem Solids*. 2006;67:1020–1023.
32. Shameli K, Ahmad MB, Yunus WMZW, et al. Synthesis and characterization of silver/talc nanocomposites using the wet chemical reduction method. *Int J Nanomedicine*. 2010;5:743–751.

33. Khanna PK, Singh N, Charan S, et al. Synthesis and characterization of Ag/PVA nanocomposite by chemical reduction method. *Mater Chem Phys*. 2005;93:117–121.
34. Song KC, Lee SM, Park TS, et al. Preparation of colloidal silver nanoparticles by chemical reduction method. *Korean J Chem Eng*. 2009; 26(1):153–155.
35. Wang H, Qiao X, Chen J, et al. Preparation of silver nanoparticles by chemical reduction method. *Colloid Surface A*. 2005;256(2–3): 111–115.
36. Jiang LP, Wang AN, Zhao Y, et al. A novel route for the preparation of monodisperse silver nanoparticles via a pulsed sonoelectrochemical technique. *Inorg Chem Commun*. 2004;7:506–509.
37. Xie Y, Ye R, Liu H. Synthesis of silver nanoparticles in reverse micelles stabilized by natural biosurfactant. *Colloid Surface A*. 2006;279: 175–178.
38. Zhang G, Chen X, Zhao J. Electrophoretic deposition of silver nanoparticles in lamellar lyotropic liquid crystal. *Mater Lett*. 2006;60: 2889–2892.
39. Andersson M, Pedersen JS, Palmqvist AEC. Silver nanoparticle formation in microemulsions acting both as template and reducing agent. *Langmuir*. 2005;21(24):11387–11396.
40. Bae DS, Kim EJ, Bang JH, et al. Synthesis and characterization of silver nanoparticles by a reverse micelle process. *Met Mater Int*. 2005;4:291–294.
41. Chen M, Feng YG, Wang X, et al. Silver nanoparticles capped by oleylamine: formation, growth, and self-organization. *Langmuir*. 2007;23(10):5296–5304.
42. Angshuman Pal, Shah S, Devi S. Microwave-assisted synthesis of silver nanoparticles using ethanol as a reducing agent. *Mater Chem Phys*. 2009;114(2–3):530–532.
43. Li K, Zhang FS. A novel approach for preparing silver nanoparticles under electron beam irradiation. *J Nanopart Res*. 2010;12:1423–1428.
44. Ahmad MB, Shameli K, Darroudi M, et al. Synthesis and characterization of silver/clay/chitosan bionanocomposites by UV-irradiation method. *Am J Appl Sci*. 2009;6(12):2030–2035.
45. Darroudi M, Ahmad MB, Shameli K, et al. Synthesis and characterization of UV-irradiated silver/montmorillonite nanocomposites. *Solid State Sci*. 2009;11:1621–1624.
46. Long D, Wu G, Chen S. Preparation of oligochitosan stabilized silver nanoparticles by gamma irradiation. *Radiat Phys Chem*. 2007;76: 1126–1131.
47. Yoksan R, Chirachanchai S. Silver nanoparticles dispersing in chitosan solution: Preparation by γ-ray irradiation and their antimicrobial activities. *Mater Chem Phys*. 2009;115:296–302.
48. Kassaee MZ, Akhavan A, Sheikh N, et al. γ-Ray synthesis of starch-stabilized silver nanoparticles with antibacterial activities. *Radiat Phys Chem*. 2008;77:1074–1078.
49. Zhu YJ, Qian Y, Li X, et al. γ-radiation synthesis and characterization of polyacrylamide-silver nanocomposites. *Chem Commun*. 1997;10: 1081–1082.
50. Bogle KA, Dhole SD, Bhoraskar VN. Silver nanoparticle: synthesis and size control by electron irradiation. *Nanotechnology*. 2006;17: 3204–3208.
51. Sheikh N, Akhavan A, Kassaee MZ. Synthesis of antibacterial silver nanoparticles by γ-irradiation. *Physica E*. 2009;42:132–135.
52. Janata E, Henglein A, Ershovt BG. First clusters of Ag^+ ion reduction in aqueous solution. *J Phys Chem*. 1994;98:10888–10890.
53. Janata E. Structure of the trimer silver clusterAg_3^{2-}. *J Phys Chem B*. 2003;107(30):7334–7336.
54. Rao YN, Banerjee D, Datta A, et al. Gamma irradiation route to synthesis of highly re-dispersible natural polymer capped silver nanoparticles. *Radiat Phys Chem*. 2010;79(12):1240–1246.
55. Kamat PV, Flumiani M, Hartland GV. Picosecond dynamics of silver nanoclusters. Photoejection of electrons and fragmentation. *J Phys Chem B*. 1998;102:3123–3128.
56. Temgire MK, Joshi SS. Optical and structural studies of silver nanoparticles. *Radiat Phys Chem*. 2004;71:1039–1044.
57. Lv Y, Liu H, Wang Z. Silver nanoparticle-decorated porous ceramic composite for water treatment. *J Membr Sci*. 2009;331: 50–56.
58. Naghavi K, Saion E, Rezaee K, et al. Influence of dose on particle size of colloidal silver nanoparticles synthesized by gamma radiation. *Radiat Phys Chem*. 2010;79:1203–1208.
59. Harekrishna B, Dipak KBi, Gobinda PS, et al. Green synthesis of silver nanoparticles using latex of *Jatropha curcas*. *Colloid Surface A*. 2009;339:134–139.
60. Huanga NM, Radimanb S, Limc HN, et al. γ-Ray assisted synthesis of silver nanoparticles in chitosan solution and the antibacterial properties. *Chem Eng J*. 2009;155(1–2):499–507.
61. Peng Chen, Linyong Song, Yankuan Liu, et al. Synthesis of silver nanoparticles by γ-ray irradiation in acetic water solution containing chitosan. *Radiat Phys Chem*. 2007;76:1165–1168.
62. Benn TM, Westerhoff P. Nanoparticle silver released into water from commercially available sock fabrics. *Environ Sci Technol*. 2008;42: 4133–4139.
63. Yang H, Du C, Jin S, et al. Preparation and characterization of SnO_2 nanoparticles incorporated into talc porous materials (TPM). *Mater Lett*. 2007;61:3736–3739.
64. Alemdar A, Güngör N, Ece ÖI, et al. The rheological properties and characterization of bentonite dispersions in the presence of non-ionic polymer PEG. *J Mater Sci*. 2005;40:171–177.
65. Gao Y, Choudhury NR, Dutta NK. Systematic study of interfacial interactions between clays and an ionomer. *J Appl Polym Sci*. 2010; 117(6):3395–3405.